Layer-resolved photoemission tomography: The *p*-sexiphenyl bilayer upon Cs doping

E. M. Reinisch, P. Puschnig, T. Ules, M. G. Ramsey, and G. Koller*
Institute of Physics, NAWI Graz, University of Graz, Universitätsplatz 5, 8010 Graz, Austria
(Received 21 December 2015; revised manuscript received 18 March 2016; published 29 April 2016)

The buried interface between a molecular thin film and the metal substrate is generally not accessible to the photoemission experiment. With the example of a sexiphenyl (6P) bilayer on Cu we show that photoemission tomography can be used to study the electronic level alignment and geometric structure, where it was possible to assign the observed orbital emissions to the individual layers. We further study the Cs doping of this bilayer. Initial Cs exposure leads to a doping of only the first interface layer, leaving the second layer unaffected except for a large energy shift. This result shows that it is in principle possible to chemically modify just the interface, which is important to issues like tuning of the energy level alignment and charge transfer to the interface layer. Upon saturating the film with Cs, photoemission tomography shows a complete doping ($6p^{4-}$) of the bilayer, with the molecular geometry changing such that the spectra become dominated by σ-orbital emissions.

DOI: 10.1103/PhysRevB.93.155438

I. INTRODUCTION

The manifold possibilities of technological applications have increased the interest in organic semiconducting materials as complement for conventional semiconductor electronics. Of particular importance to the device performance is the interface between the metal contact and the organic material. In specific, controlling the molecular geometry and the electronic level alignment of the frontier orbitals [i.e., the HOMO (highest occupied molecular orbital) and the LUMO (lowest unoccupied molecular orbital)] is a key factor for the improvement of organic device performance, i.e., minimizing the charge injection barrier and enhancing the electron transport through the organic film. Tuning of these parameters is possible via doping, which leads to charge transfer complex formation, and concomitant shifts of the molecular energy levels and the work function. Doping experiments have been performed for thick films of polymers and oligomers [1–7], and for different dopants [8–12]. However, until recently an unambiguous assignment of emissions has not been possible.

Angle-resolved ultraviolet photoemission spectroscopy (ARUPS) has been established as the prime method to investigate the electronic structure and electronic level alignment at the organic metal interface. Despite the vast literature on this theme, one should be aware of some peculiarities of ARUPS. First of all, the method is surface sensitive, i.e., the observed spectrum will be dominated by the top layer. Second, ultraviolet photoemission spectroscopy (UPS) is area averaging, i.e., nonuniform morphologies, different domains, or various layer heights will contribute according to their relative area size. Third, molecular systems have a propensity to crystalize, rather than being amorphous, which leads to distinct angular dependencies of the emitted photoelectrons and thus the chosen experimental geometry is of highest importance to correctly interpret photoemission data. For the case of multiply doped molecular species and layers, this leads to complex photoemission spectra exhibiting vast changes with emission angle, which are difficult, if not impossible, to analyze, as can be seen in the Cs exposure series of the 6P bilayer shown in Fig. 1.

A possibility to overcome these problems is the recently developed method of orbital/photoemission tomography, which allows one to identify the orbitals contributing to the spectra and also yields information on the molecular geometry. This involves interpreting the photoemission intensity map in a plane-wave final-state approximation, which yields a simple relationship between the angular distribution of the emitted electrons and the Fourier transform of the molecular orbital, from which it is emitted. The power of orbital tomography has been demonstrated in earlier works, e.g., the determination of the electronic molecular structure [13], single and multiple molecular orientations [14], geometric configurations within molecules and thin films [15,16], and substrate-enhanced modifications (dispersion) of adsorbed molecules [17,18]. In our earlier work, the strongly bound and aligned sexiphenyl (6P) monolayer on Cu(110) has been studied where we could demonstrate hybridization and LUMO occupation with orbital tomography [19]. Upon exposing this layer to an increasing amount of Cs we have observed first a decoupling of the molecular monolayer from the substrate with emptying of the hybridized LUMO, which is caused by Cs atoms diffusing through the 6P monolayer and adsorbing at the copper surface. Increasing the Cs exposure further, this is followed by refilling of the LUMO and finally the LUMO + 1 by charge transfer from the alkali metal [16]. Furthermore, the analysis of the 6P thick film showed intramolecular and intermolecular band dispersion within the organic crystal [20].

Here, we show an orbital-tomographic study of an ordered 6P bilayer on Cu(110) before and after Cs doping. We will demonstrate that it is possible to modify the electronic structure of the interfacial layer between substrate and thin film separately via Cs exposure. The observations at increasing Cs deposition range from the undoped film over filling of the 6P LUMO ($6p^{2-}$) up to filling of the LUMO + 1 ($6p^{4-}$). The focus lies (i) on the identification of the molecular features in the photoemission data, i.e., determining whether they stem from the first or second 6P layer, and (ii) the determination of the electronic structure and geometric conformation in the two layers deduced from the photoemission intensity distribution

*georg.koller@uni-graz.at

 ©2016 American Physical Society

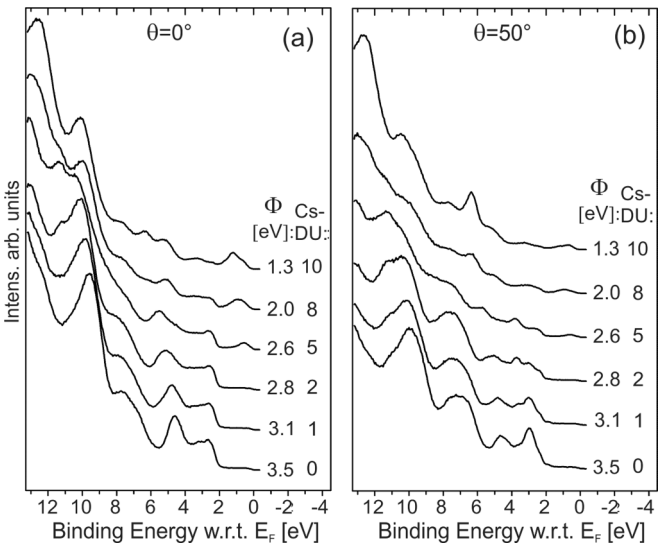

FIG. 1. He I ARUPS spectra of the 6P bilayer on Cu(110) at increasing Cs exposure from (a) normal emission (0° photoelectron takeoff angle) and (b) 50° photoelectron takeoff angle, referenced to the Fermi-level energy E_F. For each Cs dosing step the measured work function ϕ and the Cs dosing unit (DU) is indicated.

in momentum space. The experimental band and momentum maps are compared to simulations employing the plane-wave final-state approximation, which are essential to interpret the spectra correctly.

II. EXPERIMENTAL AND COMPUTATIONAL DETAILS

The Cu(110) substrate was cleaned with several cycles of Ar^+ ion sputtering and annealing at 800 K. The cleanliness of the sample was checked with low-energy electron diffraction (LEED). The growth of the 6P bilayer, which forms two complete layers on Cu(110), was monitored with a quartz microbalance. The deposition rate was kept in the range of 0.5 to 5 Å/min. Cs was deposited from a SAES getter source, applying a heating current of approximately 5 A (ac). Calibration of the deposited Cs yielded the here so-called Cs dosing unit (DU), which corresponds to approximately 0.1 Cs atom per Cu surface atom. Film growth, Cs deposition, and photoemission measurements were carried out at room temperature under UHV conditions (base pressure 10^{-10} mbar). Measurements were carried out at the Toroidal Analyzer [21] attached to the U125/2-SGM beamline at Helmholtz-Zentrum Berlin. The UV photons with an energy of $h\nu = 35$ eV had an incident angle α of 40° with respect to the substrate. The photoelectrons were collected in the plane of polarization, i.e., near the condition where the independent atomic center approximation [22–24] reduces to the plane-wave approximation result. The Toroidal Analyzer provides photoemission data in two formats: (i) Band maps show the photoelectron intensity within a selected energy window as a function of momentum parallel to the plane of incident light (=electron takeoff angles in specular geometry). Alignment of the crystal in an appropriate (often a high-symmetry) direction allows to measure the molecular band structure. (ii) Momentum maps show the momentum space (k_x,k_y) distribution at a certain energy by detecting photoelectrons from all takeoff angles in the plane of polarization while rotating the sample azimuthally. Additionally, photoemission spectroscopy and work-function measurements were made with an ADES 400 spectrometer (with a HeI UV-light source, $h\nu = 21.22$ eV).

All theoretical results presented here are obtained within the framework of density functional theory (DFT) using the VASP code [25,26]. We have performed two types of calculations: first for an isolated, undoped sexiphenyl molecule in planar geometry as well as with an inter-ring twist of 30° which is observed for 6P in the gas phase [5], and second for an isolated sexiphenyl molecule in contact with four Cs atoms. Both types of calculations were performed using a supercell with a minimum of 15 Å vacuum between the molecule's (respectively, the Cs-6P complex's) periodic replica. We employ the generalized gradient approximation (GGA) [27] for exchange-correlation effects, and the projector augmented wave (PAW) method [28] with a cutoff of about 400 eV.

The simulation of all photoemission intensity maps presented in this work is based on the one-step model of photoemission [29] where the final state is approximated by a plane wave [22]. Details of this approach are described in a recent publication [17].

Molecular adsorption geometries have been extracted from the experimental momentum via a comparison with momentum maps calculated for a range of tilt angles of the molecular plane and twisted versus planar molecular geometry (compare Fig. 2). The accuracy of the molecular tilt angle has been estimated to ±5° [16].

III. RESULTS

A. 6P bilayer on Cu(110)

A schematic of the investigated 6P bilayer structure is shown Fig. 2. It should be noted that this is not a structural model, but the molecular orientation and geometry within the layers have been inferred from the STM work by Wagner *et al.* [30] and will also be concluded from the photoemission study following. In the schematic, the 6P molecules in the first layer are planar and their long molecular axis lies parallel to the substrate and is oriented along the $[1\bar{1}0]$ surface direction. In contrast, the second-layer molecules are both tilted (average molecular plane at angle relative to substrate) and twisted (average inclination of phenyl units relative to molecular plane)

The band map and selected momentum maps at three different binding energies of a 6P bilayer on Cu(110) are presented in Fig. 3. At first glance, the photoemission band map in $[1\bar{1}0]$ direction from the 6P bilayer in Fig. 3(a) is similar to that of crystalline 6P films with either $(\bar{6}29)$ [31] or $(20\bar{3})$ [20,32] orientations and is very different from the monolayer [16,19] emissions. The band map is dominated by the intramolecular π band dispersing up from a binding energy of 8 eV at Γ to 3 eV at $k_{[1\bar{1}0]} = 1.4\,\text{Å}^{-1}$. These π emissions, arising from in total 18 orbitals, can be partitioned into three parts, i.e., the upper and lower π bands, both following the parabolic band structure (between 3 and 6 eV, and 6.5 and 8 eV binding energy, respectively) and the band of inter-ring nonbonding orbitals (HOMO-3 to HOMO-8) at 4.8 eV binding

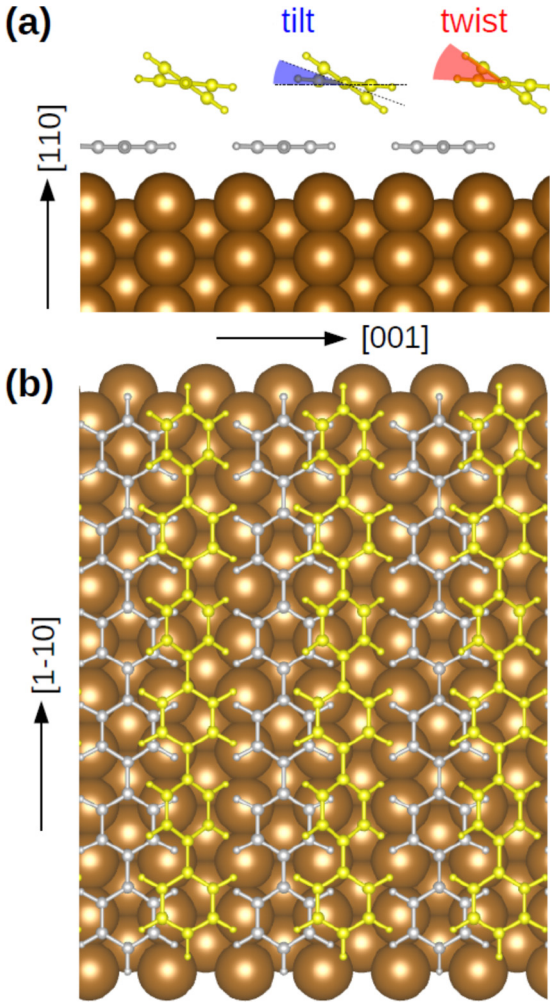

FIG. 2. Schematic of a 6P bilayer on Cu(110) in side (a) and top (b) view. Molecules in the first layer are in white, second-layer molecules are yellow. Azimuthal directions of the Cu(110) substrate are given. In (a), tilt and twist around the molecular axis are indicated.

energy, extending in $k_{[1\bar{1}0]}$ direction. These bright π-band emissions stem from molecules in the second layer. The six orbitals of the upper π band are well resolved and have a band spread of 2.9 eV, which lies between the band spreads of the planar and hybridized 6P monolayer (3.6 eV) and the 6P multilayer where the molecules are twisted (2.7 eV) [33]. This, together with the presence of the nonbonding orbitals (HOMO-3 to HOMO-8) [20] which are visible in $[1\bar{1}0]$ only for nonplanar molecules [16,24], suggests that the molecules have a twisted conformation.

The suppression of the substrate Cu d-band emissions, which normally dominate the spectra between 2 and 5 eV binding energy, suggests a complete 6P bilayer coverage. The energy region between the Fermi edge and the Cu d-band onset is reproduced at the top of Fig. 3(a) with enhanced contrast and inverted colors to emphasize weaker emissions including the Cu s,p band and molecular emissions at $E_b = 0.2\,\text{eV}/k_{[1\bar{1}0]} = 1.5\,\text{Å}^{-1}$ and $E_b = 1.9\,\text{eV}/k_{[1\bar{1}0]} = 1.35\,\text{Å}^{-1}$. Although barely visible in the band map, they are clearly confirmed by the momentum maps taken at the respective energies in Figs. 3(b)

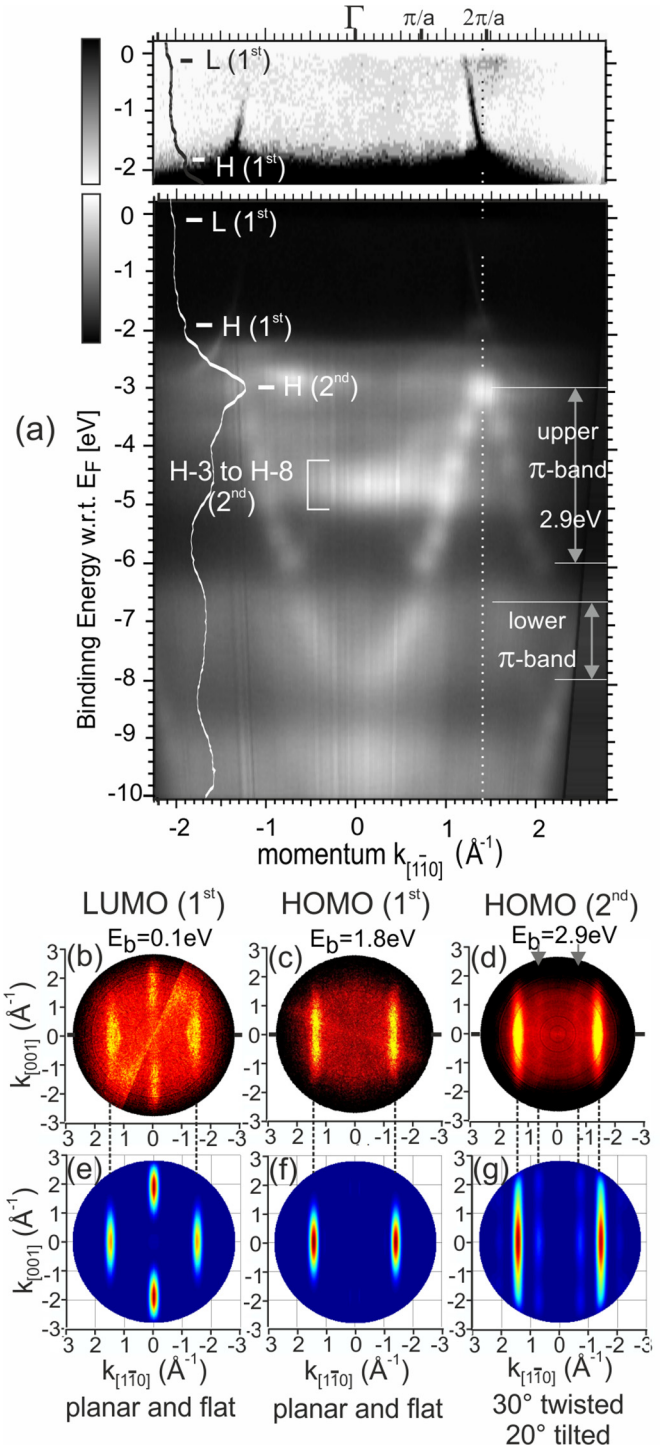

FIG. 3. ARUPS data of the 6P bilayer on Cu(110) ($h\nu = 35$ eV, $\alpha = 40°$). In the band map (a) in the $[1\bar{1}0]$ direction the energies of the hybridized LUMO (L) and HOMO (H) of the first layer, and the HOMO and nonbonding orbitals [20] (HOMO-3 to HOMO-8) of the second layer are indicated. The energy region between Fermi edge and 2 eV binding energy has been reproduced with increased intensity and inverted grayscale. The inset spectrum (white line) has been extracted from $k_{[1\bar{1}0]} = 1.4\,\text{Å}^{-1}$. The k maps (b)–(d) of the LUMO and HOMOs are compared to simulations (e)–(g) of these orbitals for the corresponding molecular conformation (first-layer molecules planar and flat, second-layer molecules twisted and tilted). The direction of the band map is indicated for each k map.

and 3(c). The binding energy and momentum values of the molecular emissions are identical to those observed for the 6P monolayer on Cu(110) [16,19,20], and they can be attributed to the partially filled 6P LUMO and HOMO of the first layer. The momentum maps of the LUMO in Fig. 3(b) and HOMO in Fig. 3(c) of the first layer are well reproduced by simulated momentum maps in Figs. 3(e) and 3(f) for planar and flat adsorbed molecules [16,22]. The appearance of LUMO emissions in the photoemission data is a result of the strong interaction of the 6P molecule with the substrate, which leads to planarization [34] of the molecules and hybridization of the LUMO with Cu surface states [19]. Together with the weak intensity they can thus be attributed to the first layer.

For the second layer, the momentum map of the emissions at the top of the π band [Fig. 3(d)) at 3.0 eV binding energy is also clearly recognizable as that of a 6P HOMO. It differs from that of the planar and flat molecule in the first layer by (i) a slight elongation of the orbital features in the $k_{[001]}$ direction induced by a molecular tilt angle and (ii) the appearance of additional features at $k_{[1\bar{1}0]} = 0.8\,\text{Å}^{-1}$ (marked with gray arrows), indicating a twisted molecular conformation [24]. The simulated momentum map in Fig. 3(g) reproduces well the measured HOMO map and suggests around $\pm 20^\circ$ tilted molecules with approximately 30° inter-ring torsional angle. The twisted (planar) conformation of this second (first) layer in the 6P bilayer is also supported by low-temperature scanning tunneling microscopy (LT-STM) studies [30].

At this point, the verification of molecular twist from photoemission data should be explained in more detail. An intramolecular twisting means an alternating torsional angle between neighboring phenyl rings along the molecular backbone. On the one hand, this leads to a lower inter-ring orbital overlap and smaller π-band spread as mentioned earlier. It also leads to a doubling of the real-space periodicity along the molecule, appearing as halved momentum space periodicity in the photoemission data. The effects of a molecular tilt and twist [22] on the momentum maps have already been illustrated for the example of the 6P ML upon doping [16]. Crystalline 6P at room temperature has been concluded to be *on average planar* from XRD, while below $110K$ it is frozen into its twisted configuration [35]. This was confirmed by ARUPS measurements, where the double periodicity of the twist is barely expressed at room temperature, while at liquid nitrogen temperature it becomes clear [20,33]. In the here presented momentum map for the second-layer HOMO in the undoped 6P bilayer in Fig. 3(d), however, the twist expresses very well, even at room temperature. This suggests that the molecules are less free to dynamically twist than in the multilayer. This probably is due to the electrostatic interaction with the substrate (including the first layer).

B. Initial doping

In a first step, the 6P bilayer system is exposed to such an amount of Cs, which is known to decouple the formerly hybridized molecules from the substrate, due to Cs adsorption at the copper surface and (re)fill the 6P LUMO with two Cs electrons ($6p^{2-}$) in the monolayer [16]. In the spectral series of Fig. 1, this would approximately correspond to a Cs exposure of 5DU. At this exposure, an emission appears 0.4 eV below E_F the LUMO-peak appears in the UPS spectra in Fig. 1. *A priori*, the development of decoupling and doping can not be assumed to happen in the interfacial layer in the 6P bilayer. The corresponding data are shown in Fig. 4, where the different developments in the two layers become apparent.

The most prominent change is that all emissions of the π band of the second layer shift 0.7 eV to higher binding energy, which is the same shift as the work-function change. This suggests that the Cs has gone to the interface and that the second layer is electrically floating on the interface potential.

Close inspection shows a new emission at the Γ point (normal emission) at 0.4 eV binding energy as can be seen in the inset with enhanced contrast in Fig. 4(a). The appearance of this LUMO emission at Γ arises from a tilt of the molecules around their molecular axes, which induces an elongation of the LUMO features along the [001] azimuthal direction visible in momentum map (b), as reported for the Cs-doped 6P monolayer [16]. This elongation of the LUMO features is reproduced by the simulation of the LUMO momentum map (d) for planar 6P tilted by $\pm 22^\circ$. The HOMO-exLUMO gap of doped 6P has been reported to be 2.1 eV [2,3,36], thus, the HOMO binding energy of the doped molecules is expected to be 2.5 eV. Due to the Cu d-band emissions starting at 2.0 eV, the HOMO emissions are not clearly recognizable in the band map. It can be concluded that the Cs has decoupled and doped the interfacial layer.

In contrast to the substantial electronic and geometric modifications in the first layer, the second layer undergoes a mere reference level shift. All second-layer emissions are still recognizable in the band map in Fig. 4(a), but are significantly shifted by 0.7 eV to higher binding energy with the HOMO (second) at 3.7 eV binding energy. This shift is dominated by a Cs-induced work-function drop. Despite this strong shift, which must bring the LUMO of the second layer very near the Fermi edge, no evidence for doping of the second layer has been found. Given the exLUMO-HOMO gap of doped 6P (2.1 eV), a filled LUMO of the second layer would be expected at around 1.6 eV binding energy, but at this binding energy no molecular emissions are found in the band map.

Compared to the second-layer HOMO of the pristine bilayer [Fig. 3(d)], the momentum space distribution of this second-layer HOMO on the doped interfacial layer [see Fig. 4(c)] has changed in the following ways: (i) The major lobes at $k_{[1\bar{1}0]} = 1.4\,\text{Å}^{-1}$ are elongated to higher $k_{[001]}$ values, which can be attributed to a slightly increased tilt angle of $\pm 20^\circ$ as suggested by the simulated HOMO momentum map in Fig. 4(e). (ii) In the region of the minor lobes at $k_{[1\bar{1}0]} = 0.8\,\text{Å}^{-1}$ which indicated the molecular twist, a mere homogeneous and relatively high background intensity is observed. The loss of features indicating the twisted configuration can presumably be understood with a dynamic twisting of the 6P molecules induced by the decoupling. The second layer interacts more weakly to the doped monolayer than to the monolayer hybridized to the substrate.

All these observations suggest that the post-deposited Cs diffuses through the top 6P layer to the substrate, where the interfacial (first) molecular layer is decoupled and doped. The geometric structure of the second-layer molecules is

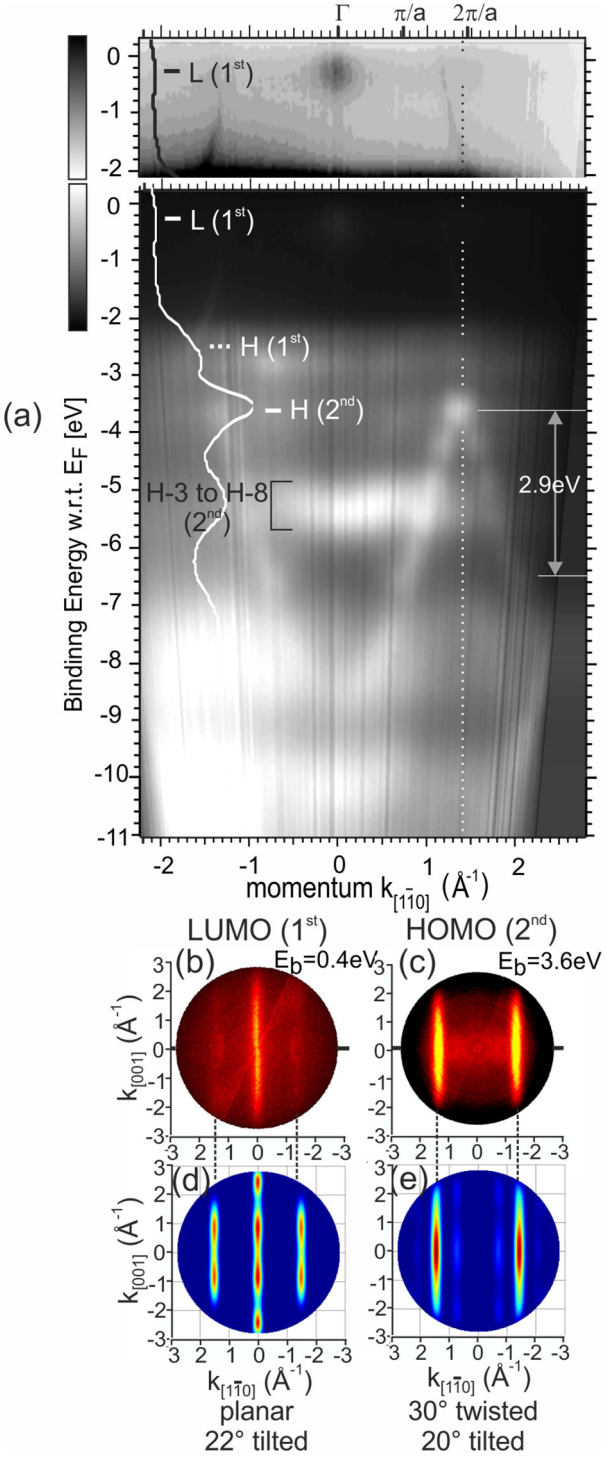

FIG. 4. ARUPS data of the 6P bilayer at initial doping ($h\nu = 35\,\mathrm{eV}, \alpha = 40^\circ$). In the band map (a) the energy positions of the first-layer LUMO, and the second-layer HOMO and nonbonding orbitals (H-3 to H-8) are labeled. The assumed energy of the first-layer HOMO is marked with a white dotted line. The energy region between Fermi edge and 2 eV binding energy has been reproduced with increased intensity. The inset spectrum has been extracted from $k_{[1\bar{1}0]} = 1.4\,\mathrm{Å}^{-1}$. The experimental momentum maps of the first-layer LUMO (b) and the second-layer HOMO (c) have been reproduced by simulated momentum maps (d), (e) with the respective geometric conformations. The direction of the band map is indicated for each k map.

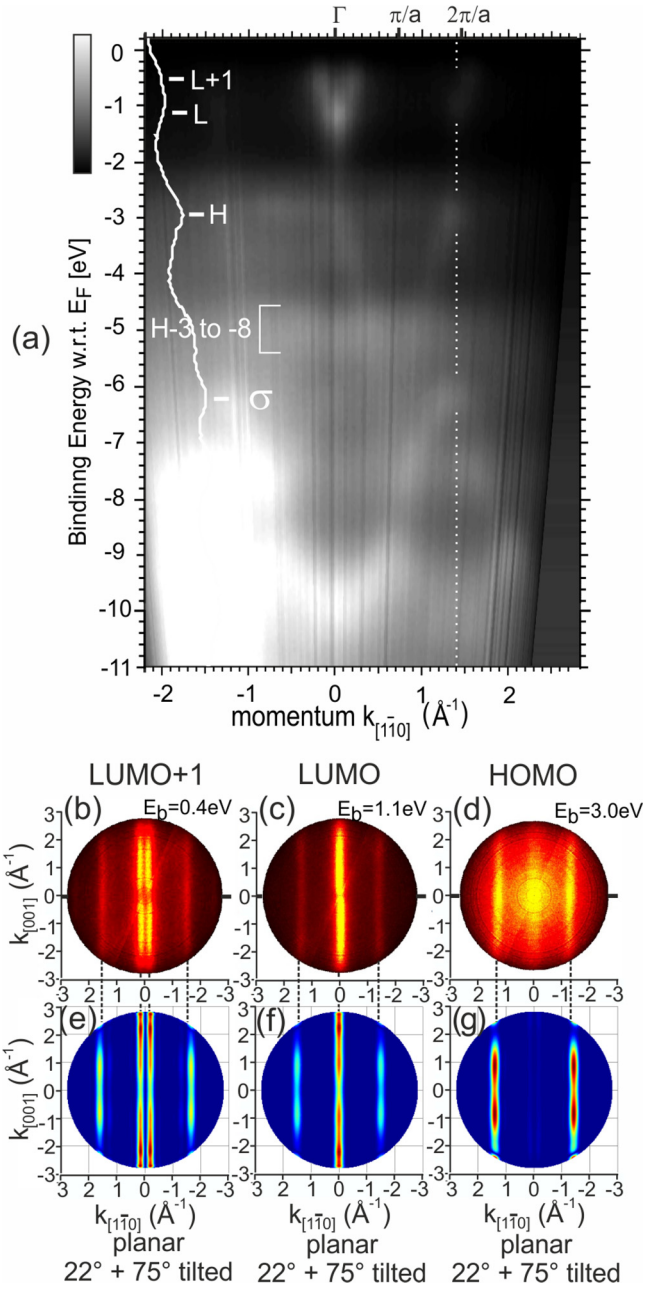

FIG. 5. ARUPS data of the quadruply doped $6p^{4-}$ bilayer ($h\nu = 35\,\mathrm{eV}, \alpha = 40^\circ$). In the band map (a) the LUMO + 1, LUMO, and HOMO energies as well as the top of an emerging σ band are labeled. The inset spectrum has been extracted from $k_{[1\bar{1}0]} = 1.4\,\mathrm{Å}^{-1}$. The measured momentum maps of the LUMO + 1 (b), LUMO (c), and HOMO (d) are reproduced by the corresponding simulated momentum maps (e) to (g) for molecules with $\pm 22^\circ$ and $\pm 75^\circ$ tilt angle. The direction of the band map is indicated for each k map.

essentially unaffected, they remain aligned along the $[1\bar{1}0]$ direction, twisted and tilted.

C. Maximum doping of the bilayer

Figure 5 shows the 6P bilayer at Cs saturation doping at room temperature. The most striking difference is the disappearance of the π-band features, which were associated with the undoped 6P second layer. In turn, we find a new bandlike

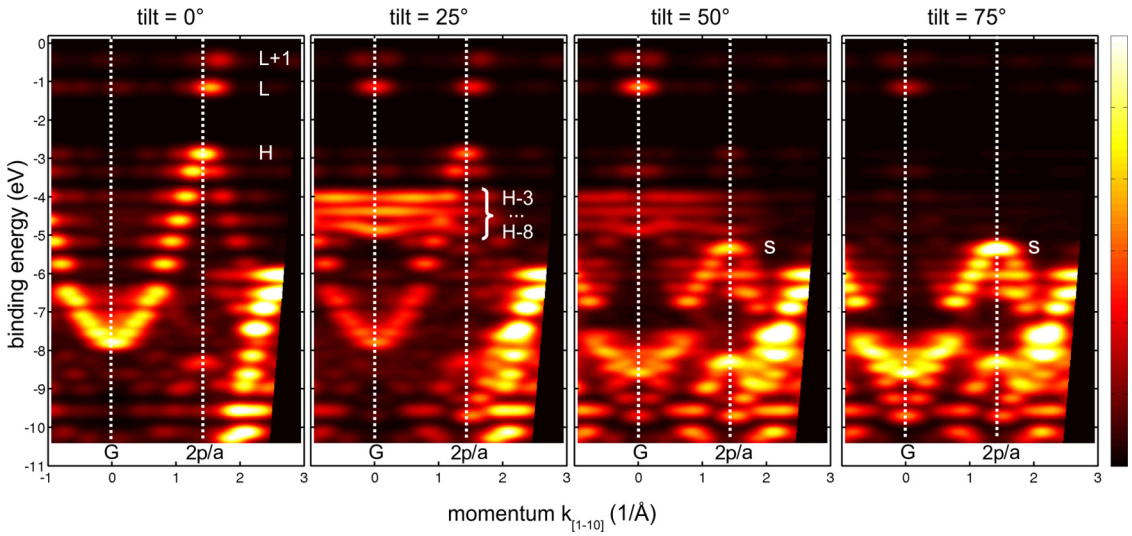

FIG. 6. Simulated GGA band maps along the long molecular axes for isolated, planar 6P molecules forming a charge transfer complex with four Cs atoms for 0°, ±25°, ±50°, and ±75° tilt angle around the long molecular axis with respect to the substrate. The most significant π-orbital emissions LUMO + 1 (L+1), LUMO (L), HOMO (H), nonbonding orbitals (H-3 to H-8), and the top of the σ band are indicated. The energies were aligned to the experimental LUMO + 1 binding energy.

structure at higher binding energies (6 to 10 eV) which will be attributed to a changed molecular geometry. Moreover, the doping-induced emissions just below the Fermi edge have become relatively intense with emissions at 0.4 and 1.1 eV. These features are attributed to filling of both LUMO and LUMO + 1, i.e., full doping and quadruply negative charging of the molecules ($6p^{4-}$) as has already been observed in the monolayer [16] and multilayer films [36]. In the band map in Fig. 5(a), the LUMO and LUMO + 1 emissions are clearly visible around Γ without need for enhancement. From the intensity distributions in the momentum maps in Figs. 5(b) and 5(c), in particular from the LUMO + 1, it is concluded that the molecules have a mixed geometry containing ±22° and ±75° tilted molecules in 1:1 ratio, as suggested by the simulated momentum maps in Figs. 5(e) and 5(f). This geometry was also observed for the quadruply doped 6P monolayer on Cu(110) [16].

The HOMO of the doped layer can now be clearly identified in the momentum maps at 3.0 eV binding energy in Fig. 5(d). It becomes easily identifiable presumably because the *entire* bilayer is doped and the Cu *d* band no longer dominates this energy region. The highly elongated HOMO emissions in the momentum map in Fig. 5(d) are reproduced by the simulated momentum map in Fig. 5(g) for a 1:1 mix of ±22° and ±75° tilted molecules.

Apart from these doping-induced states (LUMO + 1, LUMO, HOMO), there are vast changes in the band map of the fully doped 6P bilayer [Fig. 5(a)] for energies below the HOMO, such as the disappearance of the π band and the emergence of a new band, which seems difficult to identify. To this end, we have performed simulations of the photoemission band map for a quadruply doped $6p^{4-}$ where we have varied the tilt angle of the molecule from flat lying (tilt = 0°) to 75° in steps of 25°. Note that these simulations shown in Fig. 6 are based on GGA calculations and assume a plane wave as the final state of the photoemission process. While for flat lying molecules, the emissions are dominated by π-band emission, for large tilt angles, e.g. 75°, these emissions have almost disappeared while new emissions attributed to σ states of 6P dominate the band map below binding energies of 5.3 eV. We also note that the nonbonding orbitals (H-3 to H-8) are not visible for flat molecules, but show maximum photoemission intensity at low tilt angles (25°) before they vanish again for larger tilt angles. We also observe that upon increasing the tilt angle the HOMO, LUMO, and LUMO + 1 can be observed at normal emission. All these findings from the theoretical maps are in qualitative agreement with the experimental observations discussed above for the band map of the fully doped 6P bilayer shown in Fig. 5(a).

In the comparison of theory (Fig. 6) with experiment [Fig. 5(a)], the energy positions of the simulated band maps, which are based on DFT calculations at the GGA level, have been aligned to the experimental LUMO + 1 binding energy. It should be noted that the calculated band maps of Fig. 6 are also not sensitive to the exact positions of the four Cs atoms relative to the 6P molecule, as the Cs atoms merely donate their 6*s* electrons to the LUMO and LUMO + 1 orbital of 6P. Taking into account the self-interaction error of the GGA exchange-correlation functional, which is known to lead to too small binding energies for more localized states, we can attribute the emissions observed at 6.2 eV in experiment indeed to the top of the σ band of 6P. While in GGA, the top of the σ band is located at 5.5 eV binding energy, thus 2.6 eV below the HOMO (compare Fig. 6), a more sophisticated DFT calculation using the HSE hybrid functional, increases this $\pi - \sigma$ separation to 3.3 eV [37]. Thus, the top of the σ state would be located at 6.2 eV which would be in excellent agreement with experiment. As a more general aspect, the observation of the σ state in the experimental band map is remarkable because it demonstrates that the

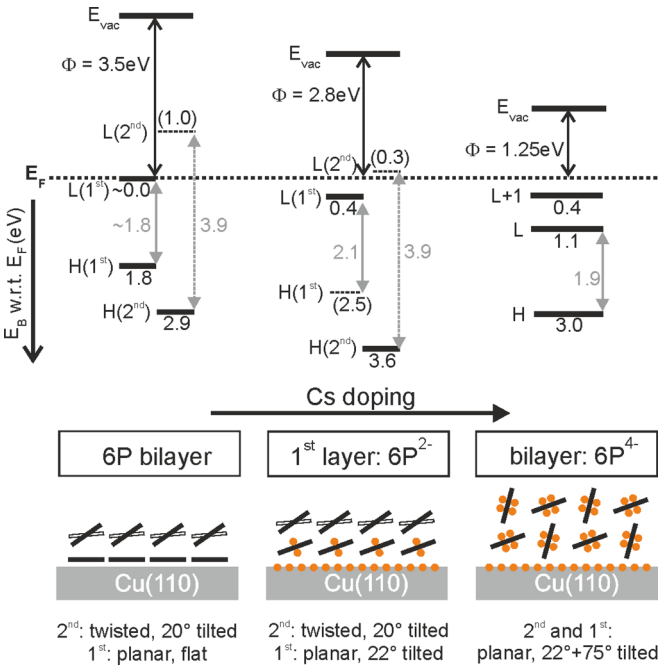

FIG. 7. Top: energy diagrams of the characteristic parameters of the 6P bilayer in the undoped, doubly doped ($6p^{2-}$), and quadruply doped ($6p^{4-}$) bilayer. Indicated are orbital binding energies for both first and second layer (with respect to the Fermi edge), work function Φ, HOMO-LUMO (transport) gap (full and dashed gray lines). The energies have been yielded by home-laboratory ARUPS measurements at room temperature. Bottom: suggested schematic of the geometric molecular configuration of the bilayer for the three investigated doping cases. The structure for the doped layers has been derived from ARUPS data, the model for the undoped case supported by LT-STM [30].

plane-wave final-state approximation also yields a reasonable description of the photoemission intensity for orbitals of σ symmetry.

In summary, the features in the entire experimental band map of the quadruply doped 6P bilayer can be identified and suggest a mix of weakly and highly tilted molecules in agreement with the LUMO and LUMO + 1 momentum map evaluation. These mixed angles suggest a herringbone structure and that doping does not cause a cofacial arrangement. Although the molecules become decoupled and modify their geometries for deposited Cs, the alignment remains along the Cu rows in [1$\bar{1}$0] direction throughout the whole Cs deposition series.

IV. DISCUSSION AND SUMMARY

By understanding the photoemission angular distribution of photoemission tomography, the emissions of the two layers of the bilayer can be distinguished and understood. This allows a summary of the development of orbital energies and the molecular geometries in the two 6P layers for the increasing Cs doping stages to be made as shown in Fig. 7.

The undoped bilayer shows a structure, where the first-layer molecules lie planar and flat on the substrate and the second-layer molecules are twisted and tilted. In the first layer of the undoped 6P bilayer, the LUMO is found at the Fermi edge suggesting fractional filling with substrate electrons. This hybridized system has a LUMO-HOMO gap of around 1.8 eV which is reduced compared to isolated neutral 6p due to screening by the additional charge on the molecule. The second-layer molecules are twisted, the simulations suggest also a ±20° tilt. In contrast to the hybridized first-layer LUMO, the LUMO of the second layer is not occupied. The energy position of the LUMO at 0.9 eV above the Fermi edge has been inferred from both a calculated electron affinity (EA) and the transport gap value of 6P. The resulting LUMO energies are consistent in both cases: (i) from the HSE-calculated EA of 2.5 eV and the measured work function of 3.5 eV, and (ii) from the HOMO-LUMO transport gap of 3.9 eV [38] (estimated from the optical gap of 3.4 eV [39] plus assumed 0.5 eV exciton binding energy) and the HOMO binding energy of 2.9 eV.

Cs doping of the first layer induces decoupling of the molecules leading to a tilt of ±20° of the molecules. The LUMO of the doped first layer is found at 0.4 eV binding energy. Of particular significance is that rather than half-filling of the LUMO of both layers, the system prefers to fully occupy the LUMO of the first layer and thus leaving the second-layer LUMO empty. The doping of the first layer leads to a change in the level alignment of the second layer, putting the LUMO close (but above E_F) without significantly changing its geometry. The undoped second layer shifts to higher binding energy in accord with the work-function drop of 0.7 eV. Such a shift would put the second-layer LUMO to close above the Fermi edge.

High Cs exposure leads to a further reduction of the work function, such that not only the LUMO, but also the LUMO + 1 are below E_F and occupied. This dramatic change in the electronic structure and the presence of four Cs atoms per molecule has not changed the orientation of the long molecular axes of the molecules. However, the molecules have adopted a higher tilt angle of the π plane, as evidenced in both the momentum maps of the π orbitals [Figs 5(b)–5(d)] and the band map [Fig. 5(a)], which is now dominated by molecular σ emissions.

We have shown that photoemission tomography can identify even strong modifications in the electronic structure of an organic/molecular base system. Photoemission tomography can thus be foreseen to become important for investigations of, for instance, sensoric systems, where similar electronic effects occur after a chemical/physical interaction.

ACKNOWLEDGMENTS

This work has been financially supported by the Austrian Science Fund (FWF), Projects No. P27427-N20 and No. P27649-N20. We thank Helmholtz Zentrum Berlin for the allocation of synchrotron radiation beam time. The research leading to these results has received funding from the European Community's Seventh Framework Programme (FP7/2007-2013) under Grant Agreement No. 312284. The computational results presented have been achieved using the Vienna Scientific Cluster (VSC).

[1] W. R. Salaneck, R. H. Friend, and J. L. Brédas, Phys. Rep. **319**, 231 (1999).

[2] M. Ramsey, D. Steinmüller, M. Schatzmayr, M. Kiskinova, and F. P. Netzer, Chem. Phys. **177**, 349 (1993).

[3] M. Ramsey, M. Schatzmayr, G. Leising, and F. P. Netzer, Mol. Cryst. Liq. Cryst. **256**, 679 (1994).

[4] C.-P. Cheng, T. Li, C.-H. Kuo, and T.-W. Pi, Org. Electron. **14**, 942 (2013).

[5] K. Seki, U. O. Karlsson, R. Engelhardt, E.-E. Koch, and W. Schmidt, Chem. Phys. **91**, 459 (1984).

[6] D. Ivory, G. Miller, J. Sowa, L. Shaklette, R. Chance, and R. Baughmann, J. Chem. Phys. **71**, 1506 (1979).

[7] M. Pfeiffer, K. Leo, X. Zhou, J. Huang, M. Hofmann, A. Werner, and J. Blochwitz-Nimoth, Org. Electron. **4**, 89 (2003).

[8] H. Mendez, G. Heimel, A. Opitz, K. Sauer, P. Barkowski, M. Oehzelt, J. Soeda, T. Okamoto, J. Takeya, J.-B. Arlin, J.-Y. Balandier, Y. Geerts, N. Koch, and I. Salzmann, Ang. Chem.: International Ed. **52**, 7751 (2013).

[9] E. E. Aziz, A. Vollmer, S. Eisebitt, W. Eberhardt, P. Pingel, D. Neher, and N. Koch, Adv. Mater. **19**, 3257 (2007).

[10] N. Koch, F. Jäckel, J. Ghijsen, M. C. Rojas, M. Grioni, J. P. Rabe, R. L. Johnson, A. Kahn, and J.-J. Pireaux, J. Electron Spectrosc. Relat. Phenom. **144-147**, 495 (2005).

[11] A. Kahn, W. Zhao, W. Gao, H. Vázquez, and F. Flores, Chem. Phys. **325**, 129 (2006).

[12] S. Olthof, S. Mehraeen, S. K. Mohapatra, S. Barlow, V. Coropceanu, J.-L. Brédas, S. R. Marder, and A. Kahn, Phys. Rev. Lett. **109**, 176601 (2012).

[13] P. Puschnig, E. M. Reinisch, T. Ules, G. Koller, S. Soubatch, M. Ostler, L. Romaner, F. S. Tautz, C. Ambrosch-Draxl, and M. G. Ramsey, Phys. Rev. B **84**, 235427 (2011).

[14] B. Stadtmüller, M. Willenbockel, E. M. Reinisch, T. Ules, F. C. Bocquet, S. Soubatch, P. Puschnig, G. Koller, M. G. Ramsey, F. S. Tautz, and C. Kumpf, Europhys. Lett. **100**, 26008 (2012).

[15] M. Wießner, D. Hauschild, A. Schöll, F. Reinert, V. Feyer, K. Winkler, and B. Krömker, Phys. Rev. B **86**, 045417 (2012).

[16] E. M. Reinisch, T. Ules, P. Puschnig, S. Berkebile, M. Ostler, T. Seyller, M. G. Ramsey, and G. Koller, New J. Phys. **16**, 023011 (2014).

[17] T. Ules, D. Lüftner, E. M. Reinisch, G. Koller, P. Puschnig, and M. G. Ramsey, Phys. Rev. B **90**, 155430 (2014).

[18] V. Feyer, M. Graus, P. Nigge, M. Wießner, R. Acres, C. Wiemann, C. Schneider, A. Schöll, and F. Reinert, Surf. Sci. **621**, 64 (2014).

[19] S. Berkebile, T. Ules, P. Puschnig, L. Romaner, G. Koller, A. J. Fleming, K. Emtsev, T. Seyller, C. Ambrosch-Draxl, F. P. Netzer, and M. G. Ramsey, Phys. Chem. Chem. Phys. **13**, 3604 (2011).

[20] G. Koller, S. Berkebile, M. Oehzelt, P. Puschnig, C. Ambrosch-Draxl, F. P. Netzer, and M. G. Ramsey, Science **317**, 351 (2007).

[21] L. Broekman, A. Tadich, E. Huwald, J. Riley, R. Leckey, T. Seyller, K. Emtsev, and L. Ley, J. Electron Spectrosc. Relat. Phenom. **144-147**, 1001 (2005).

[22] P. Puschnig, S. Berkebile, A. J. Fleming, G. Koller, K. Emtsev, T. Seyller, J. D. Riley, C. Ambrosch-Draxl, F. P. Netzer, and M. G. Ramsey, Science **326**, 702 (2009).

[23] S. Goldberg, C. Fadley, and S. Kono, Solid State Commun. **28**, 459 (1978).

[24] H. Offenbacher, D. Lüftner, T. Ules, E. M. Reinisch, G. Koller, P. Puschnig, and M. G. Ramsey, J. Electron Spectrosc. Relat. Phenom. **204A**, 92 (2015).

[25] G. Kresse and J. Hafner, Phys. Rev. B **47**, 558 (1993).

[26] G. Kresse and D. Joubert, Phys. Rev. B **59**, 1758 (1999).

[27] J. P. Perdew, K. Burke, and M. Ernzerhof, Phys. Rev. Lett. **77**, 3865 (1996).

[28] P. E. Blöchl, Phys. Rev. B **50**, 17953 (1994).

[29] P. J. Feibelman and D. E. Eastman, Phys. Rev. B **10**, 4932 (1974).

[30] M. Wagner, S. Berkebile, F. P. Netzer, and M. G. Ramsey, ACS Nano **9**, 12070 (2015).

[31] J. Novak, M. Oehzelt, S. Berkebile, M. Koini, T. Ules, G. Koller, T. Haber, R. Resel, and M. G. Ramsey, Phys. Chem. Chem. Phys. **13**, 14675 (2011).

[32] M. Oehzelt, L. Grill, S. Berkebile, G. Koller, F. P. Netzer, and M. G. Ramsey, ChemPhysChem **8**, 1707 (2007).

[33] S. Berkebile, G. Koller, P. Puschnig, C. Ambrosch-Draxl, F. P. Netzer, and M. G. Ramsey, Appl. Phys. A **95**, 101 (2009).

[34] P. Puschnig and C. Ambrosch-Draxl, Phys. Rev. B **60**, 7891 (1999).

[35] K. N. Baker, A. V. Fratini, T. Resch, H. C. Knachel, W. Adams, E. Socci, and B. Farmer, Polymer **34**, 1571 (1993).

[36] M. G. Ramsey, M. Schatzmayr, S. Stafstrom, and F. P. Netzer, Europhys. Lett. **28**, 85 (1994).

[37] P. Puschnig and D. Lüftner, J. Electron Spectrosc. Relat. Phenom. **200**, 193 (2015).

[38] J.-L. Bredas, Mater. Horizons **1**, 17 (2014).

[39] Y. Hu, K. Maschek, L. Sun, M. Hohage, and P. Zeppenfeld, Surf. Sci. **600**, 762 (2006).